Effect of damping and rotor moment of inertia on stability of self-synchronization for two unbalanced rotors

Mori, Hiroki
Department of Mechanical Engineering, Kyushu University

Sueda, Miwa
Graduate School of Science and Engineering, Saitama University

Shiroshita, Kousuke
Department of Mechanical Engineering, Kyushu University

Kondou, Takahiro
Department of Mechanical Engineering, Kyushu University

https://hdl.handle.net/2324/7167123

出版情報：Journal of Sound and Vibration. 570, pp.118103-, 2024-02-03. Elsevier
バージョン：

Effect of damping and rotor moment of inertia on stability of self-synchronization for two unbalanced rotors

Hiroki Mori*[a], Miwa Sueda[b], Kousuke Shiroshita[a], and Takahiro Kondou[a]

[a] Department of Mechanical Engineering, Kyushu University, 744 Motooka, Nishi-ku, Fukuoka 819-0395, Japan

[b] Graduate School of Science and Engineering, Saitama University, 255 Shimo-Okubo, Sakura-ku, Saitama 338-8570, Japan

Abstract

The self-synchronization of rotors in a nonlinear system has both academic and practical importance because of its applicability as a source of excitation for vibratory machines. Although the characteristics of such self-synchronization can be clarified by analyzing the periodic solutions of the equations of motion, only self-synchronization corresponding to the stable periodic solution is realized in actual systems. The stability of the solution is thus one of the most important characteristics of self-synchronization. In this paper, to stabilize periodic solutions suitable for application to vibratory machines, the effects of the damping of the rigid body and the moment of inertia of the rotors on stability are examined using a system that consists of two unbalanced rotors installed in a rigid body. High-precision analysis conducted using the shooting method shows that it is possible to stabilize the instabilities caused by period-doubling and Hopf bifurcations while keeping other characteristics, such as the synchronous frequency and the rigid body amplitude, mostly unchanged. The findings of this study can serve as a guide to extending the range of stable periodic solutions and are thus expected to be useful in the design of systems that utilize the self-synchronization of rotors.

Keywords: Self-Synchronization, Nonlinear Vibration, Stability, Shooting Method

1. Introduction

In a system where multiple nonlinear self-excited oscillators with unique frequencies are coupled, self-synchronization can occur, where all of the oscillators are entrained into a single frequency through their interactions [1-3]. In the field of mechanical vibration, the self-synchronization of pendulums [3-7] and rotors [3,8-21] has long been known, starting with the discovery of synchronization in pendulum clocks by Huygens [1]. The self-synchronization of rotors has both academic and practical importance because it can be applied as a source of excitation for vibratory machines.

The self-synchronization of rotors has several advantages. Synchronous rotation with a specific phase difference is achieved without using mechanical coupling (e.g., through chains or gears) even when there are differences in the individual characteristics of the rotors (e.g., their applied voltages). In addition, high flexibility in terms of the placement of the excitation source is obtained. To exploit these advantages in vibratory machines, it is necessary to design the system based on the characteristics of the

* Corresponding author.

E-mail addresses: hiroki@mech.kyushu-u.ac.jp (H. Mori), sueda@mail.saitama-u.ac.jp (M. Sueda), kondou.takahiro.259@m.kyushu-u.ac.jp (T. Kondou)

self-synchronization. Research has thus been conducted to elucidate these characteristics and develop analysis methods for periodic solutions of analytical models that correspond to the self-synchronization.

Zhang et al. [8] focused on the conditions that various torques, such as driving torque and damping torque, must satisfy in the synchronized state and proposed an analysis method that uses conditional equations for torques derived from an approximate analysis based on the method of averaging. The analysis method has been applied and extended to a number of systems, including a system with three rotors installed on a rigid body and synchronized in a far-resonant condition [8,9], and systems corresponding to a vibrating mill [10] and a vibrating crusher [11], each consisting of two rigid bodies and two rotors. The validity of the analytical results has also been partly confirmed through numerical simulations and experiments [9-11]. Kapitaniak et al. investigated the influence of the initial value of state variables on the self-synchronization of rotors rotating in the same direction [12] and in opposite directions [12,13] using numerical simulations, and discussed the phase difference between the rotors in the synchronized state based on the energy balance. Furthermore, for a system with many rotors coupled together, they used numerical simulations to determine the behavior of the system after the power supply to some of the rotors is cut off [14]. In addition, one study developed a tamping rammer that utilizes the self-synchronization of rotors [15].

We previously applied the shooting method to the analysis of self-synchronization in a system that consisted of two rotors, each mounted on a rigid body, and showed the effects of the stiffness of the spring that coupled the rigid bodies [16] and the characteristics of the nonlinear periodic motion of the corresponding undamped system [17] on self-synchronization. Moreover, using a system with two rotors mounted on a rigid body, we derived two conditional equations for energies that must be satisfied in the synchronized state and proposed a method for simply obtaining a periodic solution and an efficient method for examining the effects of parameters on self-synchronization [18].

These studies considered the characteristics of the self-synchronization of rotors and the development of analysis methods. Relatively little attention has been paid to the effect of parameters on the stability of the periodic solution, despite it being one of the most important characteristics in the sense that only stable solutions can actually produce self-synchronization. For high robustness against inevitable errors in machine operations, the system needs to include stable periodic solutions over a wide parameter range. To achieve this, it is useful to understand the effects of parameters on the stability of the periodic solution through an analysis that obtains all solutions, including unstable ones. Furthermore, it is desirable to develop a method that changes an unstable solution into a stable one without changing other vibration characteristics, such as frequency and amplitude.

Based on the above considerations, this study uses a system that comprises two rotating unbalanced rotors installed in a rigid body to examine the effect of the damping of the rigid body and the moment of inertia of the rotors on the stability of the periodic solution as well as on the frequency and amplitude of the rigid body. DC motors are used for the excitation of the rotor considering that the characteristics of the self-synchronization between such motors are of academic interest [16,17,19,20] and that their effectiveness has been confirmed in devices that utilize self-synchronization [15,21]. A numerical analysis is performed using the shooting method for both co-rotating and counter-rotating cases. Furthermore, based on the results, a method for stabilizing the periodic solution without affecting other characteristics is derived. Note that this paper deals with the case of two rotors rotating synchronously at a ratio of 1:1 in consideration of its importance and generality in academic and industrial fields; it does not discuss self-synchronization in which the rotors rotate at a different speed ratio [22]. In addition, although controlled synchronization using active control has been studied to achieve the desired synchronized state [23], only self-synchronization that occurs passively is considered in this paper from the viewpoint of system simplicity.

The rest of this paper is organized as follows. Section 2 presents an analytical model of the considered system and derives the equations of motion. Section 3 describes the calculation procedure in the shooting method employed for the analysis of the self-synchronization in the analytical model. Section 4 examines the effect of each parameter on the characteristics of the periodic solution, including its stability. It is demonstrated that the periodic solution can be stabilized by adjusting appropriate parameters while keeping other characteristics mostly unchanged. Section 5 summarizes the present paper.

2. Analytical model and equations of motion

Figure 1 shows the analytical model considered in this paper. This is an extension of the model used in Ref. [18], in which not only the vertical but also the horizontal degree of freedom for the rigid body is considered and the effect of gravity is included. These additions have a significant impact on the stability of self-synchronization, as shown later.

The system comprises two rotors, each of which has unbalanced masses m_1 and m_2 at distances r_1 and r_2, respectively, from the axis of rotation. The rotors are driven by DC motors, whose axes of rotation are horizontal and parallel, installed in a rigid body of mass M_b under the action of gravitational acceleration g. In the following description, the left- and right-hand motors are denoted as Motor 1 and Motor 2, respectively, and the moments of inertia of the two rotating bodies to which unbalanced masses are attached are denoted as J_{r1} and J_{r2}, respectively. The rigid body is supported by springs with spring constants k_x and k_y and dashpots with damping coefficients c_x and c_y, and is constrained to move translationally in the plane perpendicular to the motor axes and not rotate. It should be noted that a certain mechanical constraint on the rigid body rotation is introduced here, rather than the rotational degree of freedom in a rotatable system being neglected (see Appendix A for an example of such a mechanical constraint). The horizontal and vertical displacements of the rigid body are denoted as x and y, respectively, based on the static equilibrium position, and the angular displacements of Motor 1 and Motor 2 are denoted as ϕ_1 and ϕ_2, respectively. The positive directions of these variables are defined as shown in Fig. 1. Moreover, the torque constant, voltage constant, and armature resistance of the motors are denoted as K_t, K_E, and r_a, respectively, and the voltages supplied to Motor 1 and Motor 2 are denoted as e_1 and e_2, respectively. The properties of the motors are identical except for the voltages e_1 and e_2.

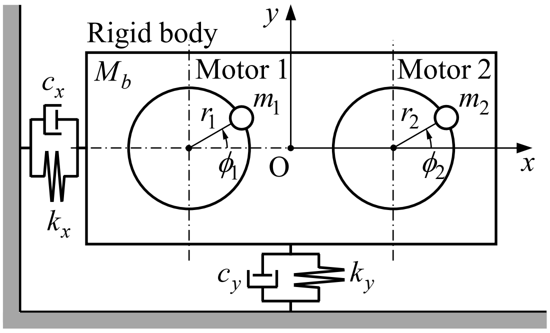

Fig. 1. Analytical model considered in this study.

With these variables, the equations of motion are derived as follows:

$$\left.\begin{aligned}
&M\ddot{x}+c_x\dot{x}+k_x x=m_1 r_1(\ddot{\phi}_1\sin\phi_1+\dot{\phi}_1^2\cos\phi_1)+m_2 r_2(\ddot{\phi}_2\sin\phi_2+\dot{\phi}_2^2\cos\phi_2)\\
&M\ddot{y}+c_y\dot{y}+k_y y=-m_1 r_1(\ddot{\phi}_1\cos\phi_1-\dot{\phi}_1^2\sin\phi_1)-m_2 r_2(\ddot{\phi}_2\cos\phi_2-\dot{\phi}_2^2\sin\phi_2)\\
&J_1\ddot{\phi}_1+B\dot{\phi}_1+m_1 g r_1\cos\phi_1=Ae_1+m_1 r_1(\ddot{x}\sin\phi_1-\ddot{y}\cos\phi_1)\\
&J_2\ddot{\phi}_2+B\dot{\phi}_2+m_2 g r_2\cos\phi_2=\sigma A e_2+m_2 r_2(\ddot{x}\sin\phi_2-\ddot{y}\cos\phi_2)
\end{aligned}\right\},\qquad (1)$$

where

$$M=M_b+m_1+m_2,\ J_1=m_1 r_1^2+J_{r1},\ J_2=m_2 r_2^2+J_{r2},\ A=\frac{K_t}{r_a},\ B=\frac{K_t K_E}{r_a},\qquad (2)$$

where A is the conversion factor between the voltages and the torques of the motors and B is the internal damping of the motors. Note that the rotational damping of the rotors is ignored under the assumption that it is sufficiently small compared to the internal damping of the motors. An overdot indicates differentiation with respect to time (i.e., $\mathrm{d}/\mathrm{d}t$). The voltages are defined to be positive (i.e., $e_1>0$ and $e_2>0$) and the two motors are co-rotating when $\sigma=1$ and counter-rotating when $\sigma=-1$.

Rescaling the time and introducing dimensionless parameters and variables, we obtain the following dimensionless system:

$$\left.\begin{aligned}
&\nu^2\xi''+2\zeta_x\nu_x\nu\xi'+\nu_x^2\xi=\mu_1\nu^2(\phi_1''\sin\phi_1+\phi_1'^2\cos\phi_1)+\mu_2\nu^2(\phi_2''\sin\phi_2+\phi_2'^2\cos\phi_2)\\
&\nu^2\eta''+2\zeta_y\nu_y\nu\eta'+\nu_y^2\eta=-\mu_1\nu^2(\phi_1''\cos\phi_1-\phi_1'^2\sin\phi_1)-\mu_2\nu^2(\phi_2''\cos\phi_2-\phi_2'^2\sin\phi_2)\\
&\alpha_1\nu^2\phi_1''+\beta\nu\phi_1'+\mu_1\nu_g^2\cos\phi_1=\varepsilon_1+\mu_1\nu^2(\xi''\sin\phi_1-\eta''\cos\phi_1)\\
&\alpha_2\nu^2\phi_2''+\beta\nu\phi_2'+\mu_2\nu_g^2\cos\phi_2=\sigma\varepsilon_2+\mu_2\nu^2(\xi''\sin\phi_2-\eta''\cos\phi_2)
\end{aligned}\right\},\qquad (3)$$

where

$$\left.\begin{array}{l}\alpha_p = \dfrac{J_p}{Mr_c{}^2},\ \ \varepsilon_p = \dfrac{A}{Mr_c{}^2\omega_c{}^2}e_p,\ \ \mu_p = \dfrac{m_p r_p}{Mr_c}\ \ (p=1,2) \\ \beta = \dfrac{B}{Mr_c{}^2\omega_c},\ \ \zeta_x = \dfrac{c_x}{2\sqrt{Mk_x}},\ \ \zeta_y = \dfrac{c_y}{2\sqrt{Mk_y}},\ \ \nu_x = \dfrac{\omega_x}{\omega_c},\ \ \nu_y = \dfrac{\omega_y}{\omega_c},\ \ \nu_g = \dfrac{\omega_g}{\omega_c},\ \ \xi = \dfrac{x}{r_c} \\ \eta = \dfrac{y}{r_c},\ \ \nu = \dfrac{\omega}{\omega_c},\ \ \omega = \dfrac{2\pi}{T},\ \ \omega_x = \sqrt{\dfrac{k_x}{M}},\ \ \omega_y = \sqrt{\dfrac{k_y}{M}},\ \ \omega_g = \sqrt{\dfrac{g}{r_c}},\ \ {}' = \dfrac{\mathrm{d}}{\mathrm{d}\tau},\ \ \tau = \omega t\end{array}\right\},\qquad (4)$$

in which T is the period of the periodic solution of Eq. (1) in the synchronized state (hereafter referred to as the synchronous solution). In addition, r_c and ω_c are the characteristic length and angular frequency, respectively, the values of which are defined depending on the purpose of the analysis (see Section 4.1 for their definitions for the analyses in this paper). Note that the dimensionless period of the synchronous solution of Eq. (3) is no longer unknown but given by 2π with the above time rescaling; instead, the dimensionless synchronous frequency ν becomes an unknown constant since the angular frequency ω of the synchronous solution is unknown.

The dimensionless system parameters and variables are as follows: α_p is the dimensionless moment of inertia, ε_p is the dimensionless voltage, μ_p is the dimensionless imbalance, β is the dimensionless internal damping of the motors, ζ_x and ζ_y are the damping ratios for the rigid body in the x and y directions, respectively, ν_x and ν_y are the dimensionless natural frequencies for the rigid body in the x and y directions, respectively, ξ and η are the dimensionless horizontal and vertical displacements, respectively, ν is the dimensionless synchronous frequency, and τ is the dimensionless time.

The characteristics of the self-synchronization of the rotors are clarified by analyzing the synchronous solution calculated from Eq. (3).

3. Application of shooting method

In order to obtain the synchronous solution, the shooting method is applied to the analytical model. Here, the synchronous solution refers to the periodic solution in which the change in the variables other than ϕ_1 and ϕ_2 becomes zero when the rotors rotate once per period (i.e., ϕ_1 and ϕ_2 are respectively increased by 2π and $2\pi\sigma$ every period). Note that the absolute values of the averages of $\dot{\phi}_1$ and $\dot{\phi}_2$ in the synchronized state thus both coincide with the synchronous angular frequency ω. The value of ν also needs to be found in the shooting method along with the initial values of the variables $\xi, \eta, \phi_1, \phi_2, \xi', \eta', \phi_1'$, and ϕ_2' for the synchronous solution. This is accomplished by a combination of numerical integration and successive approximation as follows.

The equation of motion in Eq. (3) and the variational equation for the infinitesimal variation can be written in matrix form as (see Appendix B for details)

$$\nu \mathbf{u}' = \mathbf{U}(\mathbf{u}), \tag{5}$$

$$\nu \delta \mathbf{u}' + \mathbf{u}' \delta \nu = \frac{\partial \mathbf{U}(\mathbf{u})}{\partial \mathbf{u}} \delta \mathbf{u}, \tag{6}$$

where $\mathbf{u}$ and $\delta \mathbf{u}$ are respectively the state variable vector and the variation vector defined as follows:

$$\left.\begin{aligned} &\mathbf{u} = \begin{bmatrix} \mathbf{p} \\ \nu \mathbf{p}' \end{bmatrix}, \ \delta \mathbf{u} = \begin{bmatrix} \delta \mathbf{p} \\ \nu \delta \mathbf{p}' + \mathbf{p}' \delta \nu \end{bmatrix} \\ &\mathbf{p} = [\xi \ \ \eta \ \ \phi_1 \ \ \phi_2]^T \end{aligned}\right\}. \tag{7}$$

Equations (6) and (7) consider the variation $\delta \nu$ of ν in addition to the variation $\delta \mathbf{u}$ of $\mathbf{u}$. This is because the shooting method in the present study needs to find the value of ν, in addition to the initial values of $\mathbf{p}$ and $\mathbf{p}'$, for the synchronous solution.

With the solutions of Eq. (5) at times $\tau = 0$ and $\tau = 2\pi$ denoted as $\mathbf{u}^0 = \mathbf{u}(0)$ and $\mathbf{u}^1 = \mathbf{u}(2\pi)$, respectively, the condition for the periodic solution is given by

$$\left.\begin{aligned} &\mathbf{u}^1 = \mathbf{u}^0 + \mathbf{c} \\ &\mathbf{c} = [0 \ \ 0 \ \ 2\pi \ \ 2\pi\sigma \ \ 0 \ \ 0 \ \ 0 \ \ 0]^T \end{aligned}\right\}. \tag{8}$$

The calculation of the synchronous solution in the shooting method reduces to the successive approximation of the initial value $\mathbf{u}^0$ and the dimensionless synchronous frequency ν for the solution that satisfies Eq. (8). The equations necessary for the successive approximation are derived as follows.

The general solution for the variation $\delta \mathbf{u}$ that satisfies Eq. (6) is given as (see Appendix C for details)

$$\delta \mathbf{u}(\tau) = \boldsymbol{\Psi}_u(\tau, \mathbf{u}^0, \nu) \delta \mathbf{u}^0 - \frac{\tau}{\nu^2} \mathbf{U}(\mathbf{u}) \delta \nu, \tag{9}$$

where $\delta \mathbf{u}^0 = \delta \mathbf{u}(0)$ and $\boldsymbol{\Psi}_u(\tau, \mathbf{u}^0, \nu)$ is the state transition matrix (that is, the fundamental matrix with the initial value of the identity matrix [24]) for $\delta \mathbf{u}$ for the case $\delta \nu = 0$. If $\delta \mathbf{u}^1 = \delta \mathbf{u}(2\pi)$ is used, the equation for determining the correction values $\delta \mathbf{u}_k^0$ and $\delta \nu_k$ for the initial values $\mathbf{u}_k^0$ and ν_k, respectively, in the kth iteration of the successive approximation of $\mathbf{u}^0$ and ν that satisfy Eq. (8) is derived from the equation $\mathbf{u}_k^1 + \delta \mathbf{u}_k^1 = \mathbf{u}_k^0 + \mathbf{c} + \delta \mathbf{u}_k^0$. Substituting Eq. (9) into this equation and rearranging the result yields

$$[\boldsymbol{\Psi}_u(2\pi, \mathbf{u}_k^0, \nu_k) - \mathbf{I}_{2n}] \delta \mathbf{u}_k^0 - \frac{2\pi}{\nu_k^2} \mathbf{U}(\mathbf{u}_k^1) \delta \nu_k = \mathbf{u}_k^0 - \mathbf{u}_k^1 + \mathbf{c}, \tag{10}$$

where $\mathbf{I}_{2n}$ is the $2n \times 2n$ identity matrix ($n = 4$ in the current case). Equation (10) can be used when calculating $\mathbf{u}^0$ and ν in the successive approximation.

As can be seen from Eq. (7), the initial value $\mathbf{p}^0$ of $\mathbf{p}$ is obtained from the upper half of $\mathbf{u}^0$. However, to obtain the initial value $\mathbf{p}'^0$ of $\mathbf{p}'$, an additional calculation procedure, where only the lower half of $\mathbf{u}^0$

is divided by ν, is required. To find $\mathbf{p}^0$ and $\mathbf{p}'^0$ directly without performing such a circuitous calculation via $\mathbf{u}^0$, Eq. (10) is further transformed as follows.

First, we introduce $\mathbf{q}$, defined as

$$\mathbf{q} = \begin{bmatrix} \mathbf{p} \\ \mathbf{p}' \end{bmatrix} \; (= [\xi \;\; \eta \;\; \phi_1 \;\; \phi_2 \;\; \xi' \;\; \eta' \;\; \phi_1' \;\; \phi_2']^T) \,. \tag{11}$$

The equation of motion in Eq. (3) can be written in matrix form in terms of $\mathbf{q}$ as (see Appendix D for details)

$$\mathbf{q}' = \mathbf{Q}(\mathbf{q}) \,. \tag{12}$$

In the following, in a manner similar to that for $\mathbf{u}$, $\mathbf{q}$ and its variation $\delta\mathbf{q}$ at time $\tau = 0$ ($\tau = 2\pi$) are respectively denoted as $\mathbf{q}^0$ and $\delta\mathbf{q}^0$ ($\mathbf{q}^1$ and $\delta\mathbf{q}^1$). The following relationships exist between $\mathbf{u}$ and $\mathbf{q}$, $\delta\mathbf{u}$ and $\delta\mathbf{q}$, and $\mathbf{U}(\mathbf{u})$ and $\mathbf{Q}(\mathbf{q})$:

$$\mathbf{u} = \mathbf{D}\mathbf{q} \,, \;\; \delta\mathbf{u} = \mathbf{D}\delta\mathbf{q} + \begin{bmatrix} \mathbf{0} \\ \mathbf{p}' \end{bmatrix} \delta\nu \,, \;\; \mathbf{U}(\mathbf{u}) = \nu\mathbf{D}\mathbf{Q}(\mathbf{q}) \,, \;\; \mathbf{D} = \begin{bmatrix} \mathbf{I}_n & \mathbf{0} \\ \mathbf{0} & \nu\mathbf{I}_n \end{bmatrix} . \tag{13}$$

Substituting Eq. (13) into Eq. (10) and using $\boldsymbol{\Psi}_q(\tau, \mathbf{q}^0, \nu) = \mathbf{D}^{-1}\boldsymbol{\Psi}_u(\tau, \mathbf{u}^0, \nu)\mathbf{D}$ yields the equation for determining the correction values $\delta\mathbf{q}_k^0$ and $\delta\nu_k$ for the initial values $\mathbf{q}_k^0$ and ν_k, respectively, in the k th iteration of the successive approximation of $\mathbf{q}^0$ and ν as follows:

$$[\boldsymbol{\Psi}_q(2\pi, \mathbf{q}_k^0, \nu_k) - \mathbf{I}_{2n}]\delta\mathbf{q}_k^0 + \frac{1}{\nu_k}\left([\boldsymbol{\Psi}_q(2\pi, \mathbf{q}_k^0, \nu_k) - \mathbf{I}_{2n}] \begin{bmatrix} \mathbf{0} \\ \mathbf{p}_k'^0 \end{bmatrix} - 2\pi\mathbf{Q}(\mathbf{q}_k^1) \right) \delta\nu_k = \mathbf{q}_k^0 - \mathbf{q}_k^1 + \mathbf{c} \,. \tag{14}$$

Since $\boldsymbol{\Psi}_q(2\pi, \mathbf{q}_k^0, \nu_k)$ expresses the state transition matrix for the case $\delta\nu = 0$ for the variation $\delta\mathbf{q}_k$ superimposed on the solution $\mathbf{q}_k$, which has the initial value $\mathbf{q}_k^0$, it can be directly obtained, without calculating $\boldsymbol{\Psi}_u(2\pi, \mathbf{u}^0, \nu)$, by the numerical integration of the following variational equation derived from Eq. (12) (see Appendix D for details):

$$\delta\mathbf{q}' = \frac{\partial\mathbf{Q}(\mathbf{q})}{\partial\mathbf{q}} \delta\mathbf{q} \,. \tag{15}$$

Therefore, the coefficients of $\delta\mathbf{q}_k^0$ and $\delta\nu_k$ and the right-hand side in Eq. (14) are all obtained based on Eqs. (12) and (15) without conducting any calculation for $\mathbf{u}$ using Eqs. (5) and (6).

It is noted that Eq. (3), or Eq. (12), is an autonomous system and arbitrariness exists regarding which moment within one period of a solution is set as the origin of time. To address this arbitrariness by giving the condition that defines the origin of time, the following appropriate conditional equation (scalar equation) for $\mathbf{q}^0$ is added:

$$g(\mathbf{q}^0) = 0 \,. \tag{16}$$

The equation for the successive approximation for Eq. (16) is given by

$$g(\mathbf{q}_k^0) + \frac{\partial g}{\partial \mathbf{q}^0}\delta\mathbf{q}_k^0 = 0\,. \tag{17}$$

The successive approximation that determines the correction values $\delta\mathbf{q}_k^0$ and $\delta\nu_k$ using a combination of Eqs. (14) and (17) provides the initial value $\mathbf{q}^0$ for the synchronous solution and the dimensionless synchronous frequency ν. Note that any condition that can be satisfied by the synchronous solution during one period can be used for Eq. (16) and that the characteristics of the resulting solution do not depend on the setting of this condition. An example of such a condition is that one of the displacements x and y of the rigid body or the angular displacements ϕ_1 and ϕ_2 of the rotors at $\tau = 0$ is constrained to be zero.

The stability of the synchronous solution is determined from the characteristic multiplier, i.e., the eigenvalue of $\boldsymbol{\Psi}_q(2\pi, \mathbf{q}_k^0, \nu_k)$. Theoretically, for an autonomous system, at least one of the characteristic multipliers is one and the solution is asymptotically stable if the absolute values of the other characteristic multipliers are all less than one. Otherwise, the solution is unstable.

Finally, it should be noted that since the characteristic multipliers are the eigenvalues for the state transition matrix for the variation during one period of the solution, their absolute values and corresponding eigenvectors indicate the divergence speed and vibration mode of the variation, respectively. This is the basis for the discussion in Section 4.2.3.

4. Analytical results

4.1. Results for basic parameters

In this subsection, the synchronous solution for the basic parameters given in Table 1 is obtained using the shooting method to determine the fundamental characteristics of the self-synchronization in the system shown in Fig. 1, for both the co-rotating and counter-rotating cases. The parameter values in Table 1 were determined considering the values for m_1, m_2, r_1, r_2, c_y, r_a, K_t, K_E, and e_2 for the experimental apparatus described in Ref. [16], in which two rotors are installed in a single-degree-of-freedom rigid body moving on a linear guide, and considering the ranges that the values for c_x, ω_x, ω_y, J_{r1}, J_{r2}, and e_1 can take in the system shown in Fig. 1. The characteristic length and angular frequency are set to $r_c = (r_1 + r_2)/2$ and $\omega_c = \omega_y$, respectively.

Table 1 Basic parameters of analytical model.

α_1	0.056	μ_2	0.033	ζ_x	0.025	ν_y	1
α_2	0.056	ε_2	0.012	ζ_y	0.030	ν_g	0.55
μ_1	0.033	β	0.0042	ν_x	0.7		

In the shooting method, the Runge-Kutta-Gill method is used for the numerical integration and the division number per period is set to 2048. Double-precision variables are used in the calculation and the convergence criterion in the successive approximation of the shooting method is set such that the ratio of the correction values $\delta\mathbf{q}_k^0$ and $\delta\nu_k$ to the corresponding initial values $\mathbf{q}_k^0$ and ν_k is less than 10^{-12}. It is worth noting that for the results of the shooting method shown below, it is confirmed that the successive approximation calculations converge quadratically and that one of the characteristic multipliers can be regarded to have a numerical value of exactly one within the given level of precision. The quadratic convergence indicates the appropriateness of using Newton's method to compute successive approximations in the shooting method and the latter result is consistent with the fact that Eq. (3) is an autonomous system. Therefore, the calculation procedure for the shooting method presented in Section 3 is valid and the following results can be considered to be sufficiently accurate.

The analysis is performed by varying the dimensionless voltage ε_1 supplied to Motor 1 while that (ε_2) to Motor 2 is fixed. In the calculation of the synchronous solution, the numerical solutions of $\mathbf{q}^0$ and ν obtained at a certain ε_1 are used as initial values in the successive approximation calculation for $\mathbf{q}^0$ and ν at $\varepsilon_1 \pm \Delta\varepsilon_1$, which is continuously repeated to obtain the synchronous solution branches. The results suggest that the system has three types of synchronized state, in both the co-rotating and counter-rotating cases. The synchronous solution for the co-rotating case obtained by setting $\sigma = 1$ is presented in Fig. 2, in which the three solution branches, denoted by SB_1, SB_2, and SB_3, respectively, are plotted.

The dimensionless synchronous frequency ν for all of the solution branches is shown in Fig. 2(a). The dimensionless synchronous frequency ν, the dimensionless amplitudes $\mathrm{Amp}[\xi]$ and $\mathrm{Amp}[\eta]$ for the rigid body in the x and y directions, and the average phase difference $(\sigma\phi_2 - \phi_1)_{\mathrm{ave}}$ between the rotors for each solution branch are shown in Fig. 2(b) to Fig. 2(d) for SB_1, SB_2, and SB_3, respectively. Note that the uppermost figures in Fig. 2(b) to Fig. 2(d) showing ν have different aspect ratios in order to make the shape of each solution branch clear. For convenience in the comparison with the results presented later, the values of the dimensionless moments of inertia α_1 and α_2 for the rotors and the damping ratios ζ_x and ζ_y for the rigid body are given in the figure caption. In the same manner, the synchronous solution for the counter-rotating case obtained by setting $\sigma = -1$ is presented in Fig. 3.

The solid and broken black lines represent the stable and unstable solutions, respectively, and the symbols ○, △, and ▽ on the solution branch denote the saddle-node bifurcation points, Hopf bifurcation points, and period-doubling bifurcation points, respectively. The green horizontal lines in the panel for ν represent the dimensionless natural frequencies $\nu_x (= 0.7)$ and $\nu_y (= 1)$ in the x and y directions, respectively, obtained from the model with fixed rotors, and the gray dotted horizontal line in the panel for $(\sigma\phi_2 - \phi_1)_{\mathrm{ave}}$ indicates $(\sigma\phi_2 - \phi_1)_{\mathrm{ave}} = 0$.

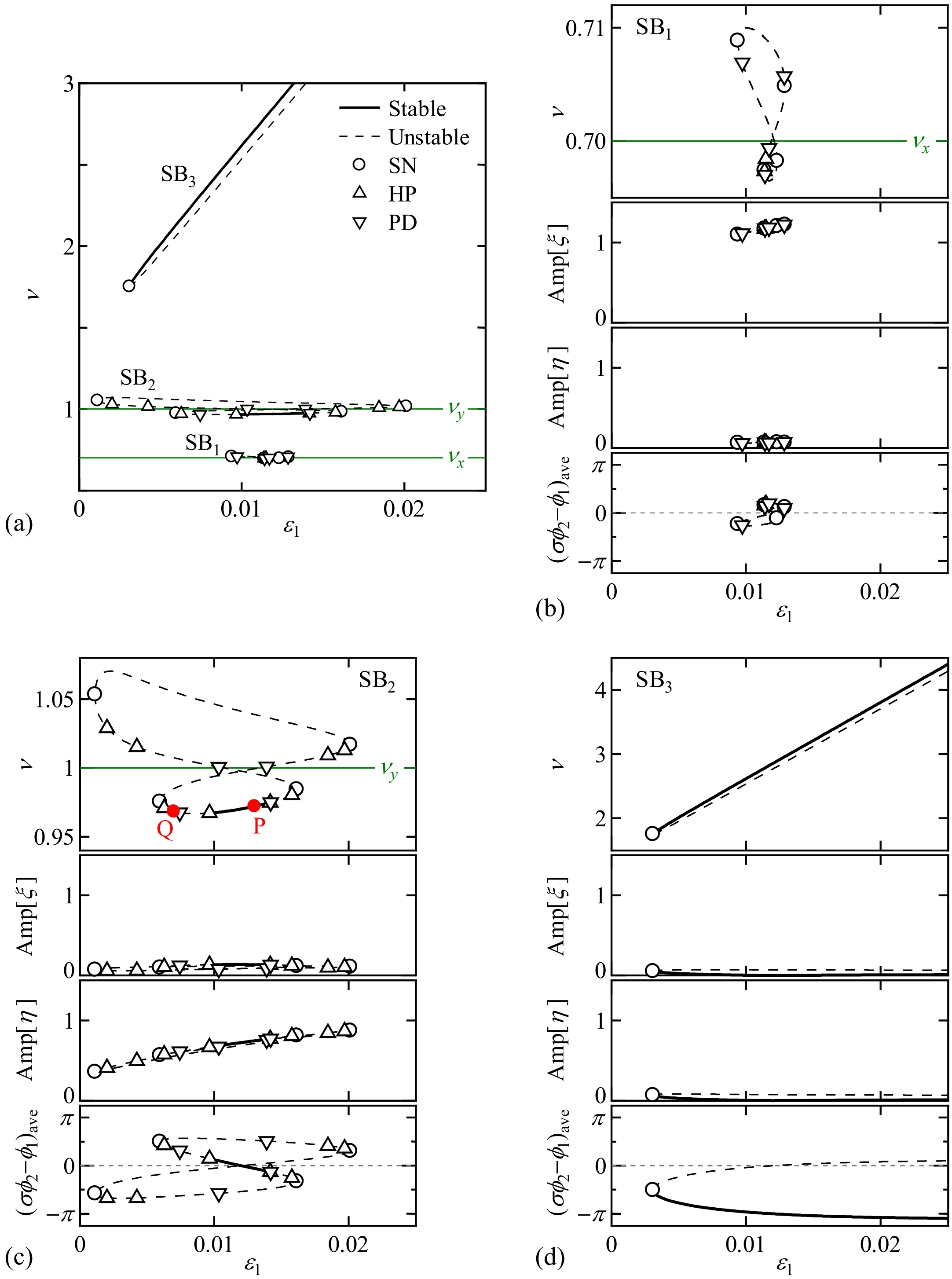

Fig. 2. Synchronous solutions for $\alpha_1 = 0.056$, $\alpha_2 = 0.056$, $\zeta_x = 0.025$, and $\zeta_y = 0.030$ for co-rotating case (SN: saddle-node, HP: Hopf, PD: period-doubling).

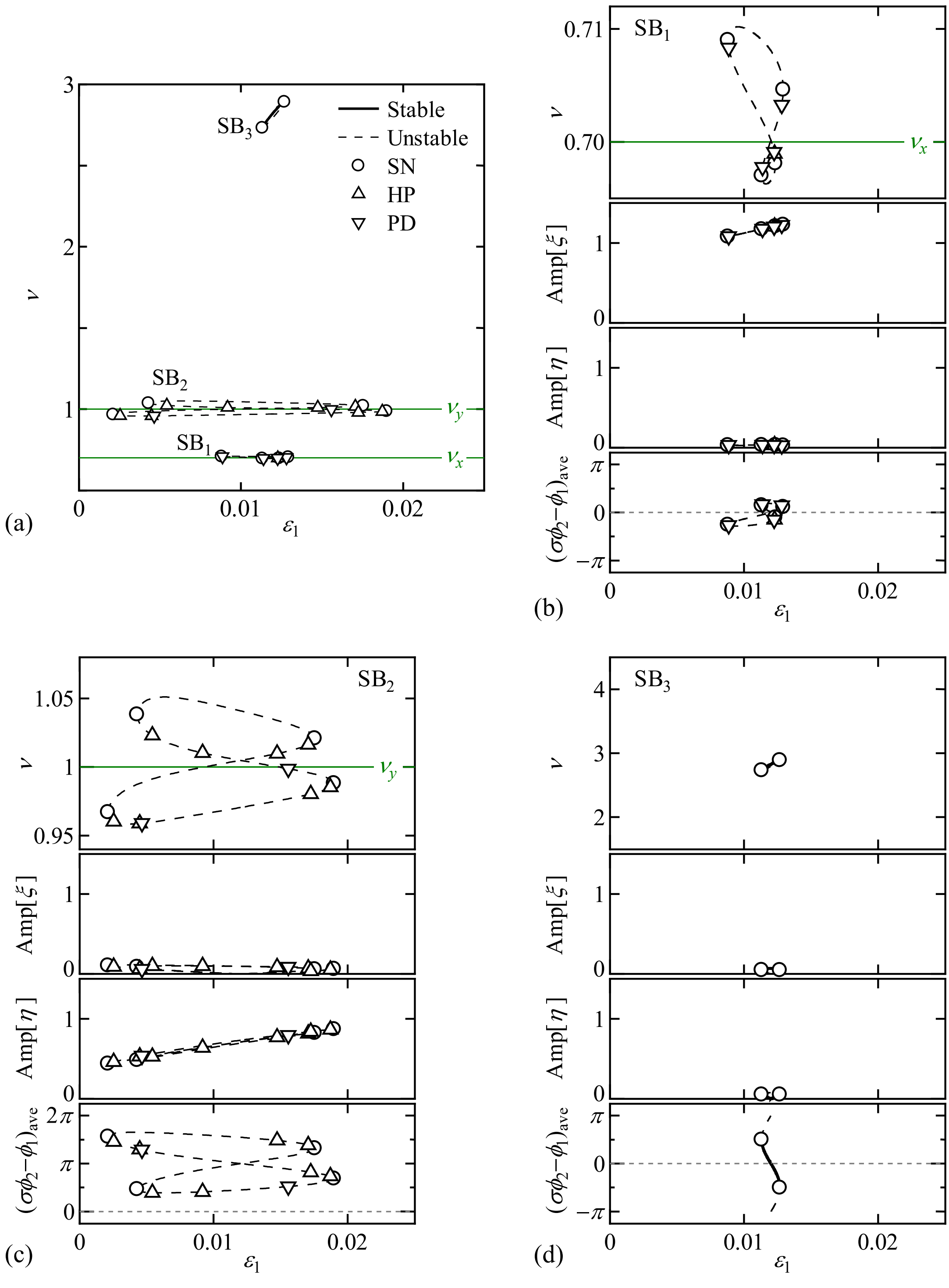

Fig. 3. Synchronous solutions for $\alpha_1 = 0.056$, $\alpha_2 = 0.056$, $\zeta_x = 0.025$, and $\zeta_y = 0.030$ for counter-rotating case (SN: saddle-node, HP: Hopf, PD: period-doubling).

1

As shown in Figs. 2 and 3, the synchronous frequency ν for SB_1 and SB_2 is close to ν_x and ν_y, respectively, and therefore the rigid body has a large amplitude in the x and y directions in SB_1 and SB_2, respectively. In contrast, ν for SB_3 is much higher than ν_x and ν_y and therefore exhibits a very small amplitude in both the x and y directions. This implies that SB_1 and SB_2 have an advantage over SB_3 in terms of efficiency when the self-synchronization of rotors is applied to a vibratory machine to produce a large vibration. On the other hand, from the viewpoint of robustness against the error in the voltage ε_1, SB_2 and SB_3 in Fig. 2 and SB_2 in Fig. 3 have an advantage over SB_1 since they extend over wide ranges for ε_1 whereas SB_1 is in a narrow range. Based on these results, the following analyses focus on the characteristics of SB_2 that are considered to have the highest significance.

Next, the stability of SB_2 is discussed. Since only self-synchronization corresponding to the stable synchronous solution is realized in actual systems, the stability of the solutions is one of the most important characteristics in both the investigation of the underlying mechanism and the application to vibratory machines. Preliminary analyses indicated that stable solutions can exist only in the bottom part of the solution branch, specifically the part between the lower two saddle-node bifurcation points, in the panels for ν in Figs. 2(c) and 3(c). However, as shown in these panels, the bottom parts of the solution branches for the basic parameters are partly and almost entirely destabilized, respectively, due to the Hopf and period-doubling bifurcations. If the applied voltage ε_1 is in the ranges for these unstable solutions, self-synchronization cannot be utilized to produce a periodic vibration of the system.

In order to demonstrate the influence of stability, the behavior of a system whose state variables are perturbed by 0.1 percent from a synchronous solution is examined at points P and Q in Fig. 2(c), which are respectively stable and unstable solutions for the co-rotating case. The results are respectively presented in Figs. 4(a) and 4(b), in which the displacements ξ and η of the rigid body and the angular velocities ϕ_1' and ϕ_2' of the rotors are shown for the interval $\tau / 2\pi = 0$ to 5, just after the perturbation is added, and for the interval $\tau / 2\pi = 195$ to 200, after a sufficient amount of time has passed.

It is confirmed from Fig. 4(a) that the system at the stable solution remains in a synchronized state with a large amplitude in the y direction even after a long period of time. In contrast, as shown in Fig. 4(b), the system at the unstable solution remains nearly synchronized just after the perturbation is added, but after a sufficient time has elapsed, the rotational velocities of the two rotors become completely desynchronized and the amplitude in the y direction, as well as that in the x direction, become small. This suggests the significance of the stability of the synchronous solution and highlights the importance of developing a method for stabilizing the unstable synchronous solution to improve the robustness in the application of self-synchronization to vibratory machines.

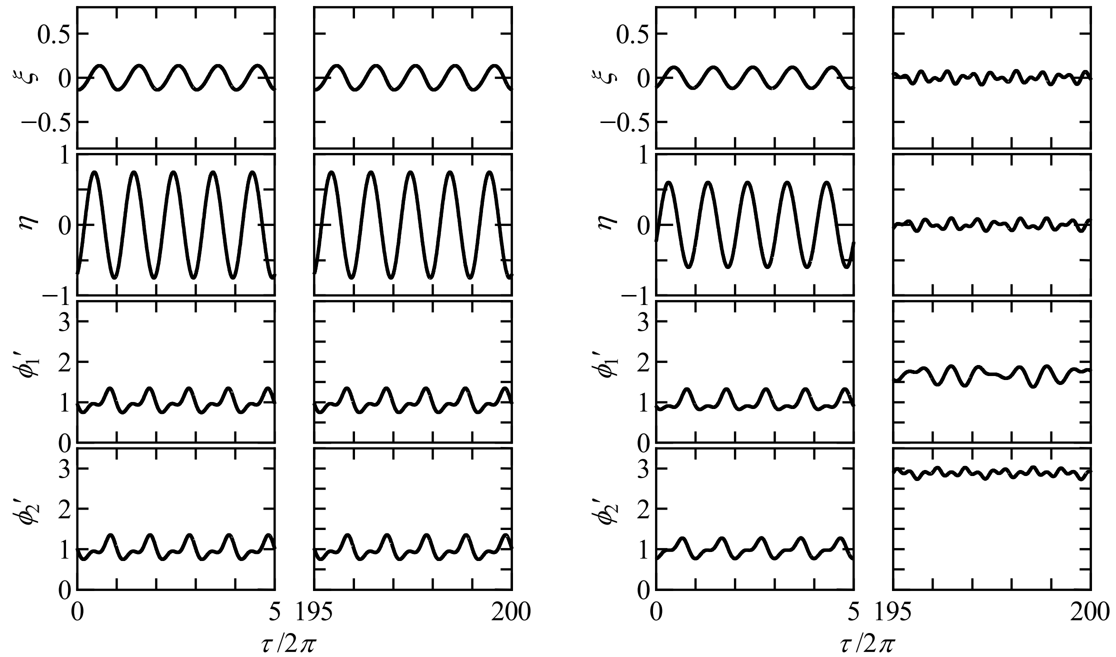

(a) Stable solution for point P at $\varepsilon_1 = 0.013$ (b) Unstable solution for point Q at $\varepsilon_1 = 0.007$

Fig. 4. Behavior of system after initial value is perturbed by 0.1 percent from synchronous solution for co-rotating case shown in Fig. 2.

4.2. Effect of parameters on stability of self-synchronization of rotors

In order to derive an effective method for stabilizing the bottom part of the synchronous solution branch SB_2 in Figs. 2(c) and 3(c), this section examines the effects of the moments of inertia α_1 and α_2 of the rotors as well as the damping ratios ζ_x and ζ_y of the rigid body on stability. In addition, their effects on the synchronous frequency ν and the amplitude $\mathrm{Amp}[\eta]$ of the rigid body in the y direction are examined as these are important vibration characteristics for SB_2.

4.2.1 Effect of damping in direction parallel to large vibration (vertical direction)

Considering that in SB_2 the amplitude of the rigid body in the y direction is much larger than that in the x direction, the damping ratio ζ_y is expected to have a significant impact on the characteristics of this solution branch. Therefore, the effect of ζ_y, or that of the damping coefficient c_y, is first examined here.

Figures 5(a) and 5(b) show the bottom part of the solution branch SB_2 obtained for $\alpha_1 = 0.056, \alpha_2 = 0.056,$ and $\zeta_x = 0.025$ in the co-rotating and counter-rotating cases, respectively. The abscissa shows the voltage ε_1 and the ordinates are the synchronous frequency ν and the amplitude $\mathrm{Amp}[\eta]$. The black, gray, red, orange, and blue lines represent the solution branches for $\zeta_y = 0.030,\ 0.035,\ 0.040,\ 0.045,$ and 0.050, respectively.

Figure 5 demonstrates that a change in ζ_y does not monotonically stabilize or destabilize the solution; instead, it influences the stability in a complex manner. Furthermore, it can be seen that the range for ε_1 where the synchronous solution exists and the amplitude $\mathrm{Amp}[\eta]$ are also significantly affected by the change in ζ_y. Therefore, a certain trial and error approach is necessary to stabilize the bottom part of SB_2 by adjusting ζ_y, and even when it can be stabilized, characteristics other than the stability are changed. This suggests that stabilizing SB_2 by adjusting ζ_y is inefficient. It is worth noting that the amplitude $\mathrm{Amp}[\xi]$ in the x direction, which is not presented here because it is less important than $\mathrm{Amp}[\eta]$, remains small in all cases of ζ_y shown in Fig. 5.

For efficiency in analysis and system design, it is desirable to control the stability without affecting other characteristics, such as the synchronous frequency, amplitude of the rigid body, and existence range of the solution. This is discussed in the following sections.

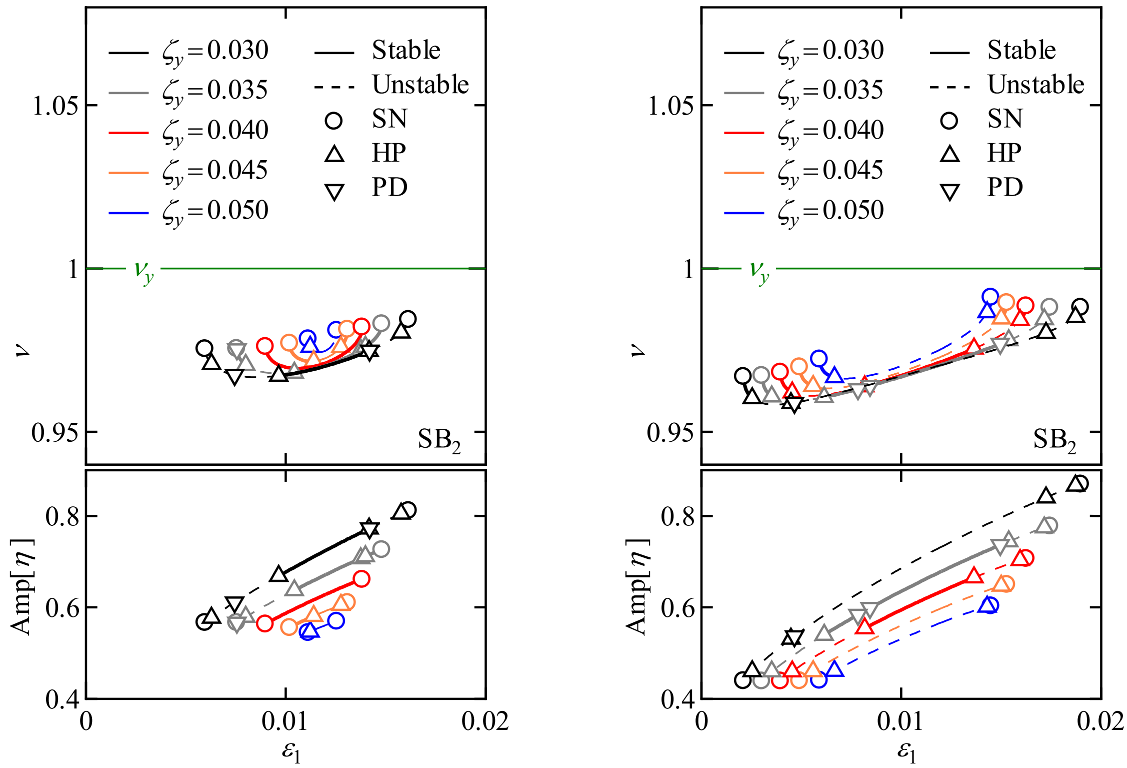

(a) Co-rotating case (b) Counter-rotating case

Fig. 5. Effect of ζ_y on bottom part of synchronous solution branch near $\nu = \nu_y$ for $\alpha_1 = 0.056$, $\alpha_2 = 0.056$, and $\zeta_x = 0.025$ (SN: saddle-node, HP: Hopf, PD: period-doubling).

4.2.2 Effect of rotor moment of inertia

To further examine the stabilization of the synchronous solution, the calculation results for the synchronous frequency ν obtained when neglecting the effect of gravity by setting $\nu_g = 0$ are presented in Fig. 6(a) for the co-rotating case and Fig. 6(b) for the counter-rotating case. Comparisons between Fig. 6(a) and Fig. 2(c) and between Fig. 6(b) and Fig. 3(c) show that the period-doubling bifurcation points vanish in Fig. 6. Considering that gravity induces a temporal variation of the rotational speed of the unbalanced rotors, it is expected that an increase in the moment of inertia of the rotors mitigates the effect of gravity and, in consequence, possibly stabilizes the instability of the synchronous solution due to the period-doubling bifurcation. Note that the synchronous frequency ν in Fig. 6 is mostly unchanged from the results shown in Figs. 2(c) and 3(c). This suggests the possibility of stabilizing the solution without changing other vibration characteristics in the synchronized state.

Based on the above consideration, the effect of the moments of inertia α_1 and α_2 of the rotors in the presence of gravity is investigated in Figs. 7(a) and 7(b), in which the synchronous frequency ν and the amplitudes $\mathrm{Amp}[\xi]$ and $\mathrm{Amp}[\eta]$ of the rigid body in the x and y directions are plotted for $\alpha_1 = \alpha_2 = 0.056, \alpha_1 = \alpha_2 = 0.060$, and $\alpha_1 = \alpha_2 = 0.070$ for the co-rotating and counter-rotating cases, respectively. Here, $\mathrm{Amp}[\xi]$ is also shown because it is next in importance to $\mathrm{Amp}[\eta]$ once the solution is stabilized. In the panel for ν, the bottom part of the solution branch is highlighted in black and the rest of the branch is plotted in gray. For simplicity, only the former black part is plotted in the panel for $\mathrm{Amp}[\xi]$ and $\mathrm{Amp}[\eta]$. Furthermore, for convenience of discussion, the period-doubling bifurcation points on the solution branch are denoted by the symbols P_1 to P_4. It should be noted that the symbols H_1 to H_8 in the rightmost panels in Figs. 7(a) and 7(b) indicate Hopf bifurcation points and are discussed in the following section.

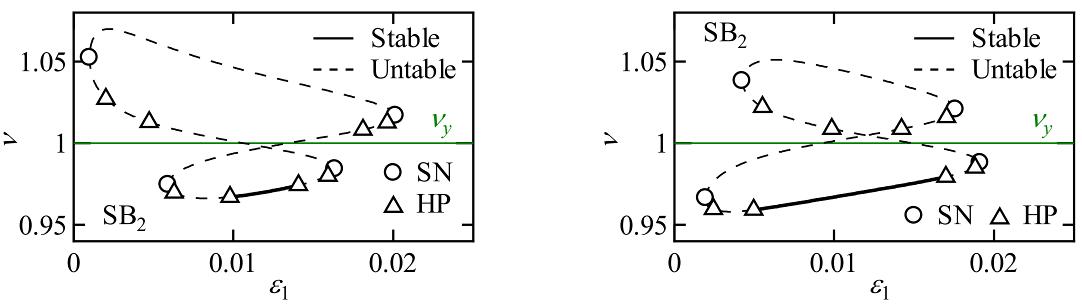

(a) Co-rotating case (b) Counter-rotating case

Fig. 6. Synchronous solution branch for ν near $\nu = \nu_y$ obtained for $\alpha_1 = 0.056, \alpha_2 = 0.056, \zeta_x = 0.025$, and $\zeta_y = 0.030$ when neglecting effect of gravity (SN: saddle-node, HP: Hopf).

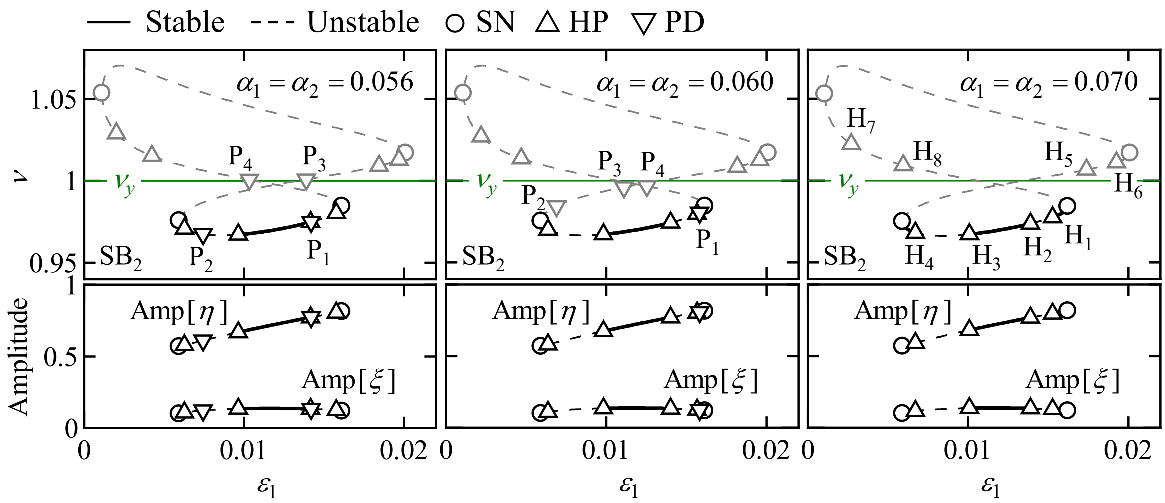

(a) Co-rotating case

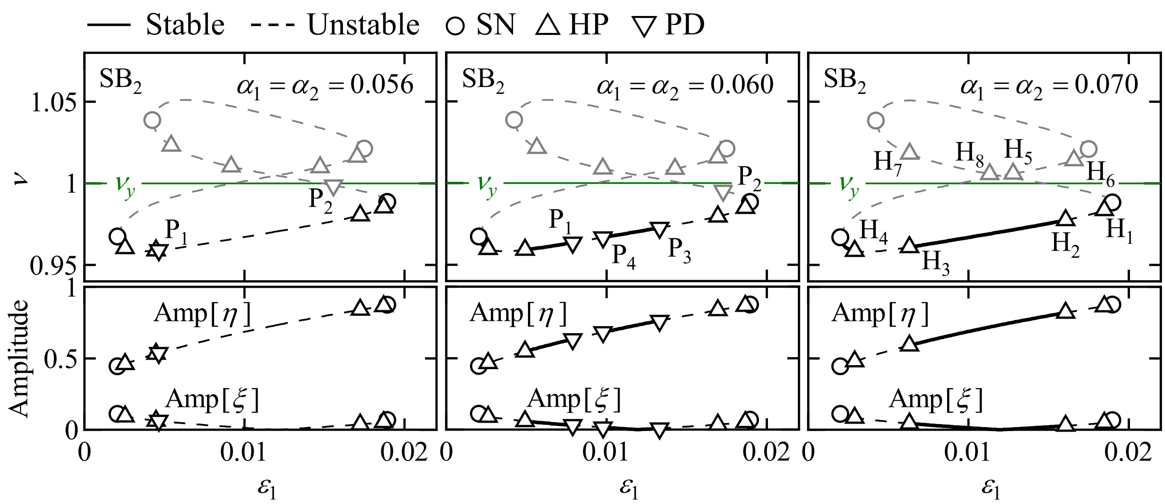

(b) Counter-rotating case

Fig. 7. Effect of α_1 and α_2 on synchronous solution for $\zeta_x = 0.025$ and $\zeta_y = 0.030$ (SN: saddle-node, HP: Hopf, PD: period-doubling, P_j $(j = 1, \ldots, 4)$ and H_j $(j = 1, \ldots, 8)$: respectively, the PD and HP bifurcation points).

Figure 7 shows that all of the period-doubling bifurcation points disappear when α_1 and α_2 are increased from 0.056 to 0.070 in both the co-rotating and counter-rotating cases, which demonstrates that the instability of the solution branch due to the period-doubling bifurcation can be stabilized by increasing the moment of inertia of the rotors. The details of the stabilization process are as follows. In the co-rotating case shown in Fig. 7(a), with an increase in α_1 and α_2 from 0.056 to 0.060, bifurcation points P_1 and P_4 and bifurcation points P_2 and P_3 move closer to each other, respectively (note that P_3 and P_4 move on the solution branch in the down-left and down-right directions, respectively, passing through an intersection in the panel for ν. Consequently, their relative left-right positioning changes after an increase in α_1 and α_2

from 0.056 to 0.060). These points coincide with each other and disappear with a further increase in α_1 and α_2 to 0.070. In the counter-rotating case shown in Fig. 7(b), on the other hand, with an increase in α_1 and α_2 from 0.056 to 0.060, a stable solution branch bounded by two bifurcation points (P_3 and P_4) appears in the interval between P_1 and P_2. Then, with a further increase in α_1 and α_2 to 0.070, points P_1 and P_4 and points P_2 and P_3 coincide with each other, respectively, and disappear.

Note that the synchronous frequency ν and the amplitudes $\mathrm{Amp}[\xi]$ and $\mathrm{Amp}[\eta]$ are mostly unchanged in Fig. 7. This means that the stabilization of the period-doubling bifurcation is achieved without changing other vibration characteristics.

4.2.3 Effect of damping in direction orthogonal to large vibration (horizontal direction)

Finally, an approach for stabilizing unstable solutions that remain in the bottom parts of the synchronous solution branches in the rightmost panels in Fig. 7, which are bounded by the Hopf bifurcation points, is discussed. Considering that the eigenvectors of the state transition matrix indicate the vibration modes of the variation (see the last paragraph in Section 3), it is expected that useful information for stabilization can be obtained by examining the eigenvector that corresponds to the characteristic multiplier responsible for the Hopf bifurcation. Based on this, as an example, the characteristic multipliers and the eigenvectors of the state transition matrix at Hopf bifurcation point H_3 in the rightmost panel in Fig. 7(a) are examined below.

Table 2 shows the characteristic multipliers for the synchronous solution at Hopf bifurcation point H_3 at $\varepsilon_1 = 0.0101$. It can be seen from Table 2 that the complex conjugate characteristic multipliers in the first and second rows are responsible for the instability due to the Hopf bifurcation. Table 3 presents the absolute values of the components in the eigenvectors, normalized to have unit norm, that correspond to the above two complex conjugate characteristic multipliers in Table 2. It can be seen that both $|\delta\xi|$ and $|\delta\xi'|$ are much larger than $|\delta\eta|$ and $|\delta\eta'|$; that is, in the vibration mode of the diverging variation, the vibration of the rigid body in the x direction is dominant. This is different to the case for the periodic solution, in which vibration in the y direction is dominant, as shown in Figs. 2(c) and 4. Therefore, the results presented in Tables 2 and 3 indicate that an increase in damping in the x direction, which suppresses the dominant vibration component of the variation, is possibly effective for the stabilization of the synchronous solution.

Next, in order to support the above consideration, the features of the aperiodic behavior of the rigid body in the unstable solution region are investigated from the viewpoint of the state variable. Figure 8 shows the vibration of the rigid body and its frequency spectrum obtained from numerical simulation at $\varepsilon_1 = 0.0095$ in the rightmost panel in Fig. 7(a), where the synchronous solution is destabilized due to Hopf bifurcation point H_3. The figure demonstrates that the frequency component close to ν_x is superimposed on ξ. In contrast, the waveform for η remains almost periodic and frequency components other than ν remain very small. These results are consistent with those shown in Tables 2 and 3, and again suggest that the instability associated with the Hopf bifurcation in Fig. 7(a) can be stabilized by increasing the damping in the x direction.

Table 2 Characteristic multipliers for synchronous solution at Hopf bifurcation point H_3 at $\varepsilon_1 = 0.0101$ in rightmost panel in Fig. 7(a).

Real part	Imaginary part	Absolute value
− 0.2414708	0.9704081	1.0000000
− 0.2414708	− 0.9704081	1.0000000
1.0000000	0.0000000	1.0000000
− 0.6021839	0.4890759	0.7757710
− 0.6021839	− 0.4890759	0.7757710
− 0.1833448	0.7315971	0.7542212
− 0.1833448	− 0.7315971	0.7542212
0.7066281	0.0000000	0.7066281

Table 3 Absolute values of eigenvector components for first and second characteristic multipliers, which are responsible for instability due to Hopf bifurcation, shown in Table 2.

$\lvert\delta\xi\rvert$	$\lvert\delta\eta\rvert$	$\lvert\delta\phi_1\rvert$	$\lvert\delta\phi_2\rvert$	$\lvert\delta\xi'\rvert$	$\lvert\delta\eta'\rvert$	$\lvert\delta\phi_1'\rvert$	$\lvert\delta\phi_2'\rvert$
0.2534	0.0282	0.1468	0.8651	0.1445	0.0749	0.0719	0.3653

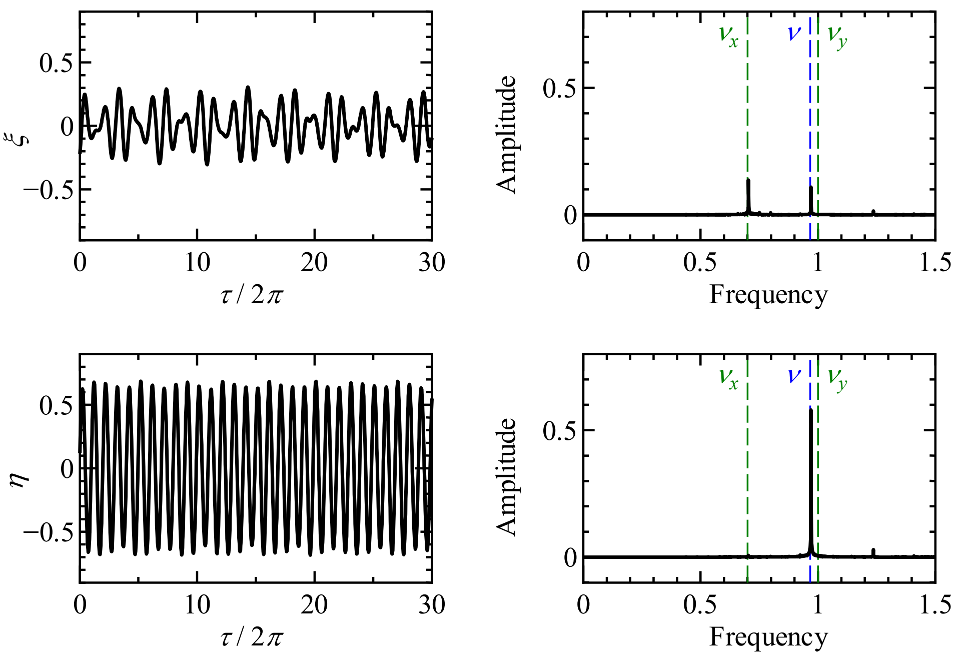

Fig. 8. Aperiodic vibration of rigid body and its frequency spectrum at $\varepsilon_1 = 0.0095$, in neighborhood of H_3, for rightmost panel in Fig. 7(a).

Based on the above, the effect of the damping ratio ζ_x, or that of the damping coefficient c_x, is investigated in Fig. 9, in which the synchronous solution is plotted for $\zeta_x = 0.025, \zeta_x = 0.045$, and $\zeta_x = 0.060$ in a manner similar to that in Fig. 7. The Hopf bifurcation points on the solution branch are denoted by the symbols H_1 to H_8. The leftmost panels in Fig. 9 are the same as the rightmost ones in Fig.

7.

Figures 9(a) and 9(b) show that all of the Hopf bifurcation points disappear as ζ_x is increased from 0.025 to 0.060, in both the co-rotating and counter-rotating cases. Therefore, as expected from the results shown in Table 2, Table 3, and Fig. 8, the instability due to the Hopf bifurcation can be stabilized by increasing the damping of the rigid body in the x direction. A careful examination of the results reveals that as ζ_x increases, Hopf bifurcation points H_1 to H_8 move on the solution branch and H_1 and H_2, H_3 and H_4, H_5 and H_6, and H_7 and H_8 respectively coincide with each other and disappear, in both the co-rotating and counter-rotating cases. Again, note that the synchronous frequency ν and the amplitudes $\mathrm{Amp}[\xi]$ and $\mathrm{Amp}[\eta]$ in Fig. 9 are mostly unchanged.

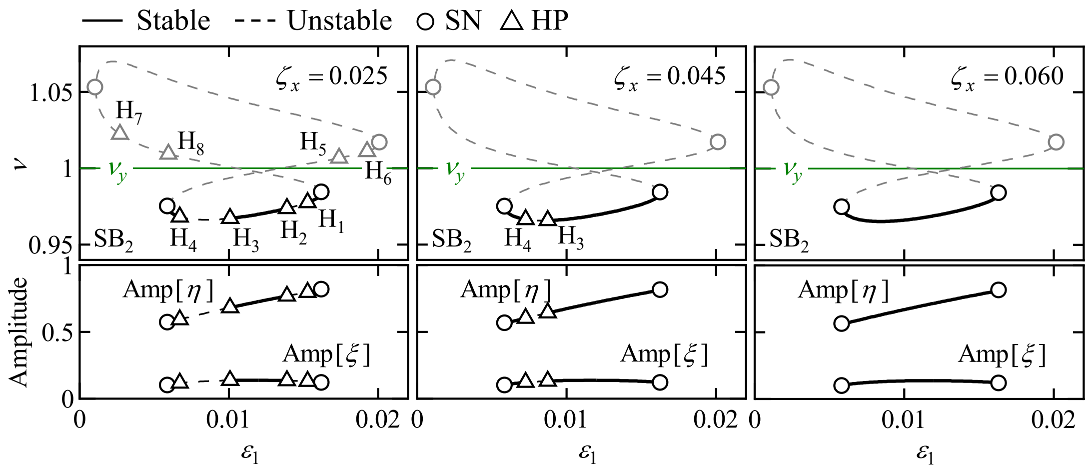

(a) Co-rotating case

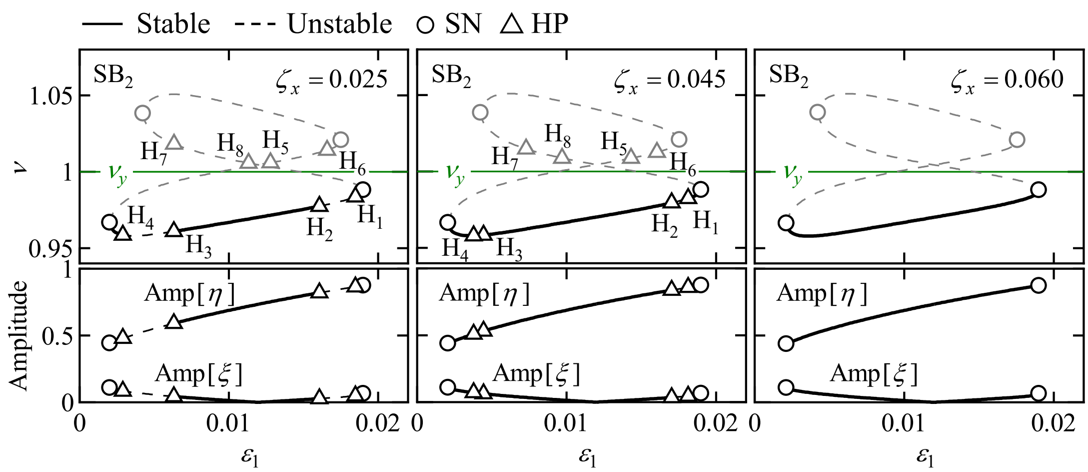

(b) Counter-rotating case

Fig. 9. Effect of ζ_x on synchronous solution for $\alpha_1 = 0.070, \alpha_2 = 0.070$, and $\zeta_y = 0.030$ (SN: saddle-node, HP: Hopf, H_j $(j = 1, \ldots, 8)$: the HP bifurcation points).

As demonstrated, an increase in α_1 and α_2 and that in ζ_x are effective for stabilizing the period-doubling and Hopf bifurcation points, and thus maximizing the range of stable solutions, in the solution branch SB_2. Since such stabilization is achieved while keeping other vibration characteristics mostly unchanged, the above findings are expected to be useful in the design of systems that utilize self-synchronization.

5. Conclusions

Stability is one of the most important characteristics of self-synchronization in both the investigation of the underlying mechanism and its application to vibratory machines. In the present study, to develop an effective method for stabilizing the synchronous solution (periodic solution), the effects of several parameters on the stability were examined using a system that comprised two unbalanced rotors installed in a rigid body that can translate in two orthogonal directions in a vertical plane.

Analyses using the shooting method suggest that the system has three types of solution branch in both the co-rotating and counter-rotating cases. One of the solution branches showed characteristics suitable for utilization in vibratory machines because the solution exists in a wide range of voltages and leads to a large vibration of the rigid body. However, it was also found that the synchronous solutions in some voltage ranges are unstable due to period-doubling and Hopf bifurcations.

To stabilize these bifurcation points, the effect of damping parallel to the large vibration of the rigid body was first examined. It was found that this damping has not only a complex effect on stability but also significant effects on other characteristics, such as the synchronous frequency and the rigid body amplitude. Next, given that the period-doubling bifurcation points do not appear when the effect of gravity is neglected, the effect of the moment of inertia of the rotors on stability was examined. The results showed that the period-doubling bifurcation points can be stabilized by increasing the rotor moments of inertia. In addition, based on the characteristics of the infinitesimal variation superimposed on the synchronous solution, the effect of damping orthogonal to the large vibration of the rigid body was investigated. It was demonstrated that the Hopf bifurcation points can be stabilized by increasing this damping. Furthermore, it was found that such stabilization of the period-doubling and Hopf bifurcations is achieved while keeping other characteristics mostly unchanged.

These findings are expected to be useful for the design and analysis of systems that utilize self-synchronization.

Acknowledgement

The authors would like to express their thanks to Mr. N. Kuboyama, Prof. N. Sowa, and Prof. T. Inoue of Kyushu University for helpful discussions. This work was supported by the Japan Society for the Promotion of Science KAKENHI [grant number JP22H01432].

Appendix A. Example of mechanical constraint on rigid body rotation

An example of the mechanical constraint for the analytical model used in this paper is shown in Fig. A.1. In this mechanism, two cross-linear guides allow two-degree-of-freedom translational motion of the rigid body while constraining its rotational motion (for simplicity, the support damping of the rigid body is not shown in the figure).

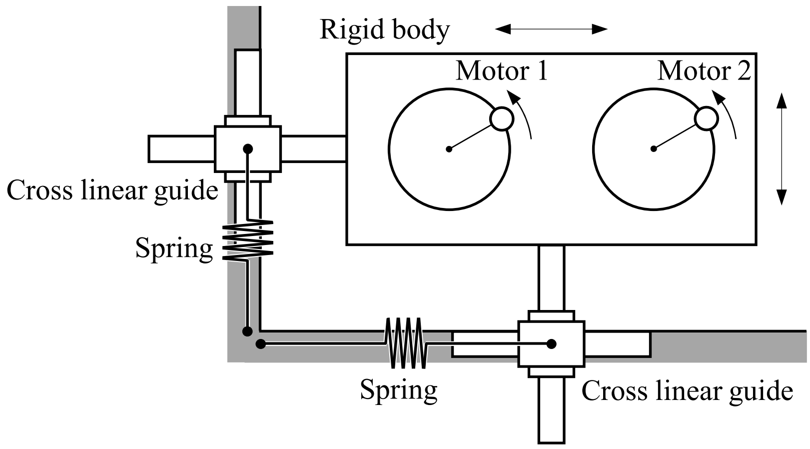

Fig. A.1. Example of mechanical constraint on rigid body rotation.

Appendix B. Transformation of Eq. (3) into Eq. (5)

This appendix shows that Eq. (3) can be transformed into Eq. (5), which is described in terms of $\mathbf{u}\ (=[u_1\ u_2\ \ldots\ u_8]^T)$ defined in Eq. (7).

First, from Eqs. (5) and (7), the components in $\mathbf{u}$ and $\mathbf{U}(\mathbf{u})\ (=[U_1\ U_2\ \ldots\ U_8]^T)$ are given by

$$u_1 = \xi\ ,\ \ u_2 = \eta\ ,\ \ u_3 = \phi_1\ ,\ \ u_4 = \phi_2\ ,\ \ u_5 = \nu\xi'\ ,\ \ u_6 = \nu\eta'\ ,\ \ u_7 = \nu\phi_1'\ ,\ \ u_8 = \nu\phi_2'\ , \tag{B.1}$$

$$U_1 = \nu\xi',\ U_2 = \nu\eta',\ U_3 = \nu\phi_1',\ U_4 = \nu\phi_2',\ U_5 = \nu^2\xi'',\ U_6 = \nu^2\eta'',\ U_7 = \nu^2\phi_1'',\ U_8 = \nu^2\phi_2''\ . \tag{B.2}$$

From Eqs. (B.1) and (B.2), the following relationships hold:

$$U_1 = u_5\ ,\ \ U_2 = u_6\ ,\ \ U_3 = u_7\ ,\ \ U_4 = u_8\ . \tag{B.3}$$

Next, Eq. (3) is written in terms of $\mathbf{u}$ and $\mathbf{U}(\mathbf{u})$ as follows:

$$\left.\begin{aligned} &U_5 - S_{u3}U_7 - S_{u4}U_8 = E_1 \\ &U_6 + C_{u3}U_7 + C_{u4}U_8 = E_2 \\ &\alpha_1 U_7 - S_{u3}U_5 + C_{u3}U_6 = E_3 \\ &\alpha_2 U_8 - S_{u4}U_5 + C_{u4}U_6 = E_4 \end{aligned}\right\}, \tag{B.4}$$

where

$$\left.\begin{array}{l} S_{u3}=\mu_1\sin u_3\ ,\ \ C_{u3}=\mu_1\cos u_3\ ,\ \ S_{u4}=\mu_2\sin u_4\ ,\ \ C_{u4}=\mu_2\cos u_4 \\ E_1=-2\zeta_x\nu_x u_5-\nu_x{}^2u_1+C_{u3}u_7{}^2+C_{u4}u_8{}^2\ ,\ \ E_2=-2\zeta_y\nu_y u_6-\nu_y{}^2u_2+S_{u3}u_7{}^2+S_{u4}u_8{}^2 \\ E_3=-\beta u_7-\nu_g{}^2C_{u3}+\varepsilon_1\ ,\ \ E_4=-\beta u_8-\nu_g{}^2C_{u4}+\sigma\varepsilon_2 \end{array}\right\}. \tag{B.5}$$

The specific expressions for U_5 to U_8, written in terms of u_1 to u_8, are obtained by solving Eq. (B.4).

Based on the above, Eq. (3) is transformed into Eq. (5) using the expressions for U_1 to U_4 given in Eq. (B.3) and the expressions for U_5 to U_8 obtained from Eq. (B.4).

Appendix C. Derivation of Eq. (9)

Since Eq. (6) is a linear differential equation in terms of $\delta\mathbf{u}(\tau)$, the general solution for $\delta\mathbf{u}(\tau)$ can be expressed as

$$\delta\mathbf{u}(\tau)=\delta\tilde{\mathbf{u}}(\tau)+\delta\hat{\mathbf{u}}(\tau), \tag{C.1}$$

where $\delta\tilde{\mathbf{u}}(\tau)$ is the general solution of the homogeneous equation, namely the equation obtained by neglecting the term with $\delta\nu$ in Eq. (6), that satisfies the initial condition of $\delta\tilde{\mathbf{u}}(0)=\delta\mathbf{u}(0)$ at time $\tau=0$, while $\delta\hat{\mathbf{u}}(\tau)$ is the particular solution of Eq. (6) that satisfies the initial condition of $\delta\hat{\mathbf{u}}(0)=\mathbf{0}$.

If $\delta\mathbf{u}(0)$ is simply represented as $\delta\mathbf{u}^0$ and the state transition matrix for $\delta\mathbf{u}$ for the case $\delta\nu=0$ is represented as $\boldsymbol{\Psi}_u(\tau,\mathbf{u}^0,\nu)$, the above solution $\delta\tilde{\mathbf{u}}(\tau)$ of the homogeneous equation is given by

$$\delta\tilde{\mathbf{u}}(\tau)=\boldsymbol{\Psi}_u(\tau,\mathbf{u}^0,\nu)\delta\mathbf{u}^0\,. \tag{C.2}$$

On the other hand, the particular solution $\delta\hat{\mathbf{u}}(\tau)$ of Eq. (6) with the initial condition $\delta\hat{\mathbf{u}}(0)=\mathbf{0}$ is given by

$$\delta\hat{\mathbf{u}}(\tau)=-\frac{\tau}{\nu^2}\mathbf{U}(\mathbf{u})\delta\nu\,. \tag{C.3}$$

It can be readily confirmed that $\delta\hat{\mathbf{u}}(\tau)$ in Eq. (C.3) satisfies $\delta\hat{\mathbf{u}}(0)=\mathbf{0}$. It also satisfies Eq. (6), as demonstrated below. Differentiating $\delta\hat{\mathbf{u}}(\tau)$ in Eq. (C.3) with respect to τ and considering Eq. (5) gives

$$\delta\hat{\mathbf{u}}'=-\frac{\mathbf{U}(\mathbf{u})}{\nu^2}\delta\nu-\frac{\tau}{\nu^2}\frac{\partial\mathbf{U}(\mathbf{u})}{\partial\mathbf{u}}\mathbf{u}'\delta\nu=-\frac{\mathbf{u}'}{\nu}\delta\nu-\frac{\tau}{\nu^2}\frac{\partial\mathbf{U}(\mathbf{u})}{\partial\mathbf{u}}\frac{\mathbf{U}(\mathbf{u})}{\nu}\delta\nu\,. \tag{C.4}$$

Considering Eq. (C.3), this is further rearranged as

$$\delta\hat{\mathbf{u}}'=-\frac{\mathbf{u}'}{\nu}\delta\nu+\frac{1}{\nu}\frac{\partial\mathbf{U}(\mathbf{u})}{\partial\mathbf{u}}\left(-\frac{\tau}{\nu^2}\mathbf{U}(\mathbf{u})\delta\nu\right)=-\frac{\mathbf{u}'}{\nu}\delta\nu+\frac{1}{\nu}\frac{\partial\mathbf{U}(\mathbf{u})}{\partial\mathbf{u}}\delta\hat{\mathbf{u}}\,. \tag{C.5}$$

Consequently, the following equation holds, demonstrating that $\delta\hat{\mathbf{u}}(\tau)$ in Eq. (C.3) satisfies Eq. (6):

$$\nu\delta\hat{\mathbf{u}}' + \mathbf{u}'\delta\nu = \frac{\partial \mathbf{U}(\mathbf{u})}{\partial \mathbf{u}}\delta\hat{\mathbf{u}} \cdot \tag{C.6}$$

Therefore, the general solution for $\delta\mathbf{u}(\tau)$ is obtained by substituting Eqs. (C.2) and (C.3) into Eq. (C.1), which results in Eq. (9).

Appendix D. Details for Eqs. (12) and (15)

This appendix shows specific expressions for the right-hand sides of Eqs. (12) and (15). The components of the vectors of interest are denoted as

$$\mathbf{q} = [q_1\ \ q_2\ \ \ldots\ \ q_8]^T\ ,\ \ \mathbf{Q}(\mathbf{q}) = [Q_1\ \ Q_2\ \ \ldots\ \ Q_8]^T\ , \tag{D.1}$$

$$\delta\mathbf{q} = [\delta q_1\ \ \delta q_2\ \ \ldots\ \ \delta q_8]^T\ ,\ \ \frac{\partial \mathbf{Q}(\mathbf{q})}{\partial \mathbf{q}}\delta\mathbf{q} = [Q_{1\delta}\ \ Q_{2\delta}\ \ \ldots\ \ Q_{8\delta}]^T\ . \tag{D.2}$$

First, $Q_i\ (i = 1, 2, \ldots, 8)$ is expressed as

$$\left.\begin{array}{l} Q_1 = q_5\ ,\ \ Q_2 = q_6\ ,\ \ Q_3 = q_7\ ,\ \ Q_4 = q_8 \\ Q_5 = \dfrac{N_1}{D_q}\ ,\ \ Q_6 = \dfrac{N_2}{D_q}\ ,\ \ Q_7 = \dfrac{N_3}{D_q}\ ,\ \ Q_8 = \dfrac{N_4}{D_q} \end{array}\right\}, \tag{D.3}$$

where

$$\left.\begin{array}{l} D_q = \alpha_1\alpha_2\nu^8 - \alpha_1\mu_2{}^2\nu^8 - \alpha_2\mu_1{}^2\nu^8 + \mu_1{}^2\mu_2{}^2\nu^8\sin^2(q_3 - q_4) \\ N_1 = \alpha_1\alpha_2\nu^6 E_1 - \mu_1\mu_2\nu^4(C_{q4}E_3 - C_{q3}E_4)\sin(q_3 - q_4) \\ \qquad - \alpha_1\nu^2(C_{q4}{}^2E_1 + C_{q4}S_{q4}E_2 - \nu^2 S_{q4}E_4) - \alpha_2\nu^2(C_{q3}{}^2E_1 + C_{q3}S_{q3}E_2 - \nu^2 S_{q3}E_3) \\ N_2 = \alpha_1\alpha_2\nu^6 E_2 - \mu_1\mu_2\nu^4(S_{q4}E_3 - S_{q3}E_4)\sin(q_3 - q_4) \\ \qquad - \alpha_1\nu^2(C_{q4}S_{q4}E_1 + S_{q4}{}^2E_2 + \nu^2 C_{q4}E_4) - \alpha_2\nu^2(C_{q3}S_{q3}E_1 + S_{q3}{}^2E_2 + \nu^2 C_{q3}E_3) \\ N_3 = -\mu_2{}^2\nu^6 E_3 + \mu_1\mu_2\nu^6 E_4\cos(q_3 - q_4) - \mu_1\mu_2\nu^4(C_{q4}E_1 + S_{q4}E_2)\sin(q_3 - q_4) \\ \qquad + \alpha_2\nu^4(S_{q3}E_1 - C_{q3}E_2 + \nu^2 E_3) \\ N_4 = -\mu_1{}^2\nu^6 E_4 + \mu_1\mu_2\nu^6 E_3\cos(q_3 - q_4) + \mu_1\mu_2\nu^4(C_{q3}E_1 + S_{q3}E_2)\sin(q_3 - q_4) \\ \qquad + \alpha_1\nu^4(S_{q4}E_1 - C_{q4}E_2 + \nu^2 E_4) \end{array}\right\}, \tag{D.4}$$

with

$$\left.\begin{array}{l} C_{q3} = \mu_1\nu^2\cos q_3\ ,\ \ S_{q3} = \mu_1\nu^2\sin q_3\ ,\ \ C_{q4} = \mu_2\nu^2\cos q_4\ ,\ \ S_{q4} = \mu_2\nu^2\sin q_4 \\ E_1 = -2\zeta_x\nu_x\nu q_5 - \nu_x{}^2 q_1 + C_{q3}q_7{}^2 + C_{q4}q_8{}^2\ ,\ \ E_2 = -2\zeta_y\nu_y\nu q_6 - \nu_y{}^2 q_2 + S_{q3}q_7{}^2 + S_{q4}q_8{}^2 \\ E_3 = -\beta\nu q_7 - \mu_1\nu_g{}^2\cos q_3 + \varepsilon_1\ ,\ \ E_4 = -\beta\nu q_8 - \mu_2\nu_g{}^2\cos q_4 + \sigma\varepsilon_2 \end{array}\right\}. \tag{D.5}$$

Next, $Q_{i\delta}$ $(i=1, 2, \ldots, 8)$ is expressed as

$$\left.\begin{array}{l} Q_{1\delta}=\delta q_5\ ,\ Q_{2\delta}=\delta q_6\ ,\ Q_{3\delta}=\delta q_7\ ,\ Q_{4\delta}=\delta q_8 \\ Q_{5\delta}=\dfrac{N_{1\delta}}{D_q}\ ,\ Q_{6\delta}=\dfrac{N_{2\delta}}{D_q}\ ,\ Q_{7\delta}=\dfrac{N_{3\delta}}{D_q}\ ,\ Q_{8\delta}=\dfrac{N_{4\delta}}{D_q} \end{array}\right\}, \tag{D.6}$$

where the expressions for $N_{1\delta}, N_{2\delta}, N_{3\delta}$, and $N_{4\delta}$ are given by replacing the E_1 to E_4 included in N_1, N_2, N_3, and N_4, previously shown in Eq. (D.4), by the following $E_{1\delta}$ to $E_{4\delta}$:

$$\left.\begin{array}{l} E_{1\delta}=-2\zeta_x \nu_x \nu\delta q_5-\nu_x{}^2\delta q_1+2C_{q3}q_7\delta q_7+(C_{q3}q_7{}'-S_{q3}q_7{}^2)\delta q_3+2C_{q4}q_8\delta q_8+(C_{q4}q_8{}'-S_{q4}q_8{}^2)\delta q_4 \\ E_{2\delta}=-2\zeta_y \nu_y \nu\delta q_6-\nu_y{}^2\delta q_2+2S_{q3}q_7\delta q_7+(S_{q3}q_7{}'+C_{q3}q_7{}^2)\delta q_3+2S_{q4}q_8\delta q_8+(S_{q4}q_8{}'+C_{q4}q_8{}^2)\delta q_4 \\ E_{3\delta}=-\beta\nu\delta q_7+(C_{q3}q_5{}'+S_{q3}q_6{}'+\mu_1\nu_g{}^2\sin q_3)\delta q_3 \\ E_{4\delta}=-\beta\nu\delta q_8+(C_{q4}q_5{}'+S_{q4}q_6{}'+\mu_2\nu_g{}^2\sin q_4)\delta q_4 \end{array}\right\}. \tag{D.7}$$

References

[1] A. Pikovsky, M. Rosenblum, J. Kurths, Synchronization (A universal concept in nonlinear sciences), Cambridge University Press, 2001.

[2] J.W.S. Rayleigh, The Theory of Sound, vol. 2, Dover Publications, 1945, pp. 221-222.

[3] I.I. Blekhman, Synchronization in Science and Technology. ASME Press, New York, 1988.

[4] V. Jovanovic, S. Koshkin, Synchronization of Huygens' clocks and the Poincaré method, J. Sound Vib. 331(12) (2012) 2887-2900.

[5] M. Senator, Synchronization of two coupled escapement-driven pendulum clocks, J. Sound Vib. 291(3-5) (2006) 566-603.

[6] J.P. Ramirez, R.H.B. Fey, K. Aihara, H. Nijmeijer, An improved model for the classical Huygens' experiment on synchronization of pendulum clocks, J. Sound Vib. 333(26) (2014) 7248-7266.

[7] M. Kapitaniak, K. Czolczynski, P. Perlikowski, A. Stefanski, T. Kapitaniak, Synchronization of clocks, Phys. Rep. 517(1-2) (2012) 1-69.

[8] X. Zhang, B. Wen, C. Zhao, Synchronization of three non-identical coupled exciters with the same rotating directions in a far-resonant vibrating system, J. Sound Vib. 332(9) (2013) 2300-2317.

[9] X. Zhang, B. Wen, C. Zhao, Experimental investigation on synchronization of three co-rotating non-identical coupled exciters driven by three motors, J. Sound Vib. 333(13) (2014) 2898-2908.

[10] X. Zhang, H. Yue, Z. Li, J. Xu, B. Wen, Stability and coupling dynamic characteristics of a vibrating system with one internal degree of freedom and two vibrators, Mech. Syst. Signal Process. 143 (2020) 106812.

[11] X. Zhang, B. Wen, C. Zhao, Vibratory synchronization transmission of a cylindrical roller in a vibrating mechanical system excited by two exciters, Mech. Syst. Signal Process. 96 (2017) 88-103.

[12] M. Kapitaniak, K. Czolczynski, P. Perlikowski, A. Stefanski, T. Kapitaniak, Synchronous states of slowly

rotating pendula, Phys. Rep. 541(1) (2014) 1-44.

[13] K. Czolczynski, P. Perlikowski, A. Stefanski, T. Kapitaniak, Synchronization of pendula rotating in different directions, Commun. Nonlinear Sci. Numer. Simul. 17(9) (2012) 3658-3672.

[14] M. Kapitaniak, M. Lazarek, M. Nielaczny, K. Czolczynski, P. Perlikowski, T. Kapitaniak, Synchronization extends the life time of the desired behavior of globally coupled systems, Sci. Rep. 4 (2014) 4391.

[15] Y. Bonkobara, T. Ono, T. Kondou, Development of a Generation Mechanism of Synchronous Vibration Suitable for Hand-Held Vibrating Tools: Investigation of an Impact Model with Two Oscillators, J. Syst. Des. Dyn. 5(6) (2011) 1361-1375.

[16] Y. Bonkobara, H. Mori, T. Kondou, T. Ayabe, Self-synchronization Phenomena Generated in Rotor-Type Oscillators: On the Influence of Coupling Condition between Oscillators, J. Syst. Des. Dyn. 2(3) (2008) 861-873.

[17] H. Mori, Y. Bonkobara, T. Kondou, T. Ayabe, Self-Synchronized Phenomena Generated in Rotor-Type Oscillators: Investigation Using Nonlinear Normal Modes, J. Syst. Des. Dyn. 2(3) (2008) 874-885.

[18] M. Sueda, H. Mori, T. Kondou, Analytical study of self-synchronization in two unbalanced rotors based on energetic conditions, J. Sound Vib. 521 (2022) 116618.

[19] J.M. Balthazar, J.L.P. Felix, R.M. Brasil, Some comments on the numerical simulation of self-synchronization of four non-ideal exciters, Appl. Math. Comput., 164(2) (2005) 615-625.

[20] A.A.N. Djanan, B.R.N. Nbendjo, P. Woafo, Effect of self-synchronization of DC motors on the amplitude of vibration of a rectangular plate, Eur. Phys. J. Spec. Top. 223 (2014) 813-825.

[21] T. Kondou, H. Mori, Y. Bonkobara, T. Ayabe, Moving apparatus utilizing a self-synchronized phenomenon, Trans. Jpn. Soc. Mech. Eng. C, 71(712) (2005) 3351-3358 (in Japanese).

[22] X. Zhang, X. Zhang, W. Hu, W. Zhang, W. Chen, Z. Wang, B. Wen, Theoretical, numerical and experimental studies on multi-cycle synchronization of two pairs of reversed rotating exciters, Mech. Syst. Signal Process. 167 (2022) 108501.

[23] Á. Miklós, Z. Szabó, Simulation and experimental validation of the dynamical model of a dual-rotor vibrotactor, J. Sound Vib. 334 (2015) 98-107.

[24] A. P. Seyranian, A. A. Mailybaev, Multiparameter Stability Theory with Mechanical Applications, Vol.13, World Scientific, Singapore, 2003.